C: Physical Processes in Nanomaterials and Nanostructures

Experimental and Ab Initio Studies of Deep-Bulk Traps in Doped Rare-Earth Oxide Thick Films

Leandro Silva Rosa Rocha, Federico Schipani, Celso Manuel Aldao, Luís A. Cabral, Alexandre Z. Simoes, Carlos Eugenio Macchi, Gilmar Eugenio Marques, Miguel Adolfo Ponce, and Elson Longo

J. Phys. Chem. C, **Just Accepted Manuscript** • DOI: 10.1021/acs.jpcc.9b07217 • Publication Date (Web): 03 Dec 2019

Experimental And A*b Initio* Studies Of Deep-Bulk Traps In Doped Rare-Earth Oxide Thick Films

Leandro S. R. Rocha[1*], Federico Schipani[2], Celso M. Aldao[2], Luis Cabral[3], Alexandre Z. Simoes[4], Carlos Macchi[5], Gilmar E. Marques[3], Miguel A. Ponce[1,2], Elson Longo[1]

[1] Federal University of São Carlos, Department of Chemistry, São Carlos, Brazil.
[2] Institute of Materials Science and Technology (INTEMA), University of Mar Del Plata and National Research Council (CONICET), Mar Del Plata, Argentina.
[3] Department of Physics, Federal University of São Carlos 13565-905, São Carlos, Sp, Brazil.
[4] São Paulo State University (UNESP), School of Engineering, Guaratinguetá, Brazil.
[5] Instituto de Física de Materiales Tandil (UNCPBA) and CIFICEN (UNCPBA-CICPBA-CONICET), Tandil, Argentina

ABSTRACT Lanthanum-doped CeO_2 is a promising semiconductor for gas sensing. A combined study applying impedance spectroscopy and first-principle calculations was performed for pure and lanthanum-doped samples. The results showed a strong influence of the localized Ce 4f states on the electrical conduction processes, and an electrical resistance increase, as a function of the exposure to vacuum and air atmospheres. After its modification with a rare-earth element along with exposure to reducing and oxidizing atmospheres, the observed behavior suggested the presence of multi-traps, which depended on the described equilibrium between the oxygen vacancies ($V_o^x \leftrightarrow V_O^{\cdot} \leftrightarrow V_O^{\cdot\cdot}$) in a disordered deep-bulk trap location. According to the DFT results, the multi-traps were formed with the creation of an oxygen vacancy far from the

doping atom. They were considered to be responsible for the phenomena modifying the Debye-like response. The transfer of electrons from Ce(III) to the adsorbed oxygen species, decreasing the number of electrons in the 4f state, reduced the electrical conductivity by the hopping frequency dependence of the total resistance and capacitances. This was probably owing to the interactions between defective oxygen and metallic species.

1. Introduction

Nanostructured rare-earth doped semiconductor oxides have attracted tremendous attention due to potential for multifunctional applications, ranging from solid oxide fuel cells (SOFC) [1] to gas sensors [2] and photo-catalysts [3]. In fact, doped ceria (CeO_2) is one of the most attractive rare-earth oxides particularly owing to its high ionic conductivity at relatively low temperatures (< 800 °C) [4] combined with high a chemical stability [5], advancing its use in various fields.

Monocrystalline CeO_2 crystallizes as a fluorite structure (Fm-3m) and presents a band gap (E_g) of 6eV (O 2p → Ce 5d), as measured by optical reflectance [6], with oxygen vacancies ($V_O^{\bullet\bullet}$) as the predominant ionic defects [7]. Doping CeO_2 with low valence compounds introduces oxygen vacancies in the structure along with a slight distortion in the local structure [8], playing an important role in determining its overall physico-chemical properties. Indeed, a study of the ionic conductivity of CeO_2 doped with different rare-earth elements suggested that rare-earth doping plays multiple roles in increasing the oxygen vacancies [9]. Because of this modification, the Ce 4f states can be occupied or unoccupied, with a redox (reduction/oxidation) process of $Ce^{+4} \rightarrow Ce^{+3}$. The ionic nature of the oxygen vacancies plays a key part in its capability to reduce or increase its oxidation state because the step that controls the redox rate, the oxygen diffusion, depends on its type, size, and concentration [10]. This indicates that different processing conditions

may favor the formation of more desired oxygen vacancies, thereby resulting in distinct improved properties, intrinsically related to its applicability. Hence, understanding these vacancies and defects is required.

In dealing with rare-earth oxides with 4f-shells, we must consider the presence of localized states at the semiconductor band gap. In addition, the presence of ionized oxygen vacancies as the predominant defects in these non-stoichiometric systems must be considered. These vacancies, which donate electrons to the localized states at the semiconductor band gap, are also responsible for the generation of small polarons. A small polaron is a defect created when an electronic carrier becomes trapped at a given site because of the displacement of adjacent species. The entire defect (carrier plus distortion) then migrates via an activated hopping mechanism. This phenomenon can occur in materials whose conduction electrons belong to incomplete inner (d or f) shells, which display a slight electron wave-function overlap and tend to form extremely narrow bands. The presence of electrons in these localized states leads to an electrical conduction based on the hopping mechanism [11,12]. Non-stoichiometric oxides such as PrO_{3-x}, TbO_{2-x}, and CeO_{2-x}, which have fluorite-type structures, are interesting semiconductors, with their x-composition varying over a wide range (from 0 to 0.5) with reduction, i.e., with the control of the oxygen partial pressure (pO_2) during the synthesis [13]. In addition, CeO_2 has the following two advantages over other oxides:

a) it offers the best opportunity to achieve the theoretically simple case where the x-concentration of electrons is small;

b) its electronic structure is simple because the Ce^{4+} species in CeO_2 has an empty 4f shell that starts to become occupied only under redox processes.

Therefore, the removal of oxygen species donates electrons to the bulk of the semiconductor as well as generates ionized oxygen vacancies in the structure, such as V_O^x, $V_O^{\cdot}$, $V_O^{\cdot\cdot}$, depicted as multi-traps, as represented in Figure 1, which shows the possible oxygen

vacancies diffusion paths, their interactions between couples of vacancies and with the surrounding atmosphere, as well as structural relaxations around vacancies. This process of oxygen vacancy generation also creates small polarons, responsible for the hopping conduction mechanism.

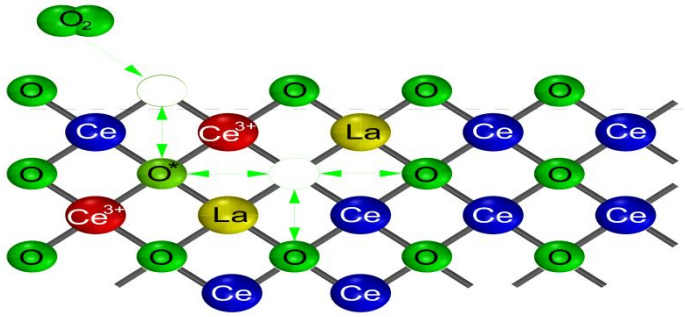

Figure 1 – Schematic of the multi-traps, represented as oxygen vacancy sites neighboring Ce(III) species.

Studies by Blumenthal et al. [14,15] indicated that hopping-type conductivity indeed occurred in reduced (CeO_{2-x}) ceria-based systems. In the first investigation [14], they attempted to hold x constant by purging the system with purified He gas but found that the readings changed with time and therefore, was necessary to heat or cool the sample relatively rapid to avoid changes in the composition. They reported a hopping activation energy (Ea) of 0.22eV at a low x, which increased with increasing x. In the second study [15], the conductivity was measured in equilibrium as a function of pO_2 and compared with separately determined thermogravimetric data for x vs pO_2. They claimed that this second method yielded better results than the previous non-equilibrium method and reported a slightly smaller value of Ea = 0.16eV (compared to the first case) for mildly reduced CeO_2.

The valence band of pure CeO_2 is primarily composed of O 2p states, whereas the conduction band is predominantly formed by Ce 5d states, with a narrow Ce 4f band in between. The current understanding is that the full Ce 4f states are localized atomic f-like species located at the neighboring vacancies of the cerium atoms (i.e. the three-dimensional electronic density suggests a higher probability of the electron to be found on its first-neighboring oxygen

vacancy). Although their exact separation is still not clear, it is suggested that the 4f occupied states may be anywhere in the range of 1.5 – 2.5eV above the valence band energy (E_v) [16]. This occupancy in the final state may change owing to the charge transfer from valence or conduction bands because of doping, which is a general phenomenon in Ce-based compounds, implying mixed valences of both $4f^0$ and $4f^1$ configurations [17]. Additionally, the modification with rare-earth elements promotes oxygen donation by lowering the necessary energy to form surface anionic vacancies when exposed to a gaseous atmosphere. Subsequently, the two excess electrons are located on the structural species, reducing them to Ce(III) and La(II), once stable mononuclear La(II) compounds can be found [18]. The rare-earth doping also favors the activation of O_2 molecules on the surface of oxygen vacancies, leading to the formation of a superoxide (O_2^-) radical as well as re-oxidation of Ce(III) to Ce(IV) [19].

We have previously reported the optimization regarding the synthesis of pure CeO_2, in terms of distinct mineralizer agents (2M KOH, NaOH, and NH_4OH) [20] followed by the evaluation of the influence of distinct synthesis times (1, 2, 4 and 8 min) on its microstructural and photoluminescent (PL) properties [21]. Then, the modification with rare-earth elements was also studied with respect to the addition of Lanthanum [La(III)] species at 4, 8 and 12wt% in terms of XRD and Rietveld refinement, Raman, UV-Vis and PL spectroscopies along with SEM analysis [22]. The main goal of lanthanum addition was to induce the creation of defective species causing structural expansion [23], resulting in the improvement of the gas sensing properties. The electrical behavior of the pure ceria-based films obtained from the powders synthesized at distinct soaking times was also investigated in the presence of 200mmHg (0.263atm) of synthetic air and CO atmospheres, in a temperature ranging from 100 °C to 350°C. Afterwards, the temperature of 350°C was kept, changing the CO and Air atmosphere pressures for 10 (0.013atm), 50 (0.065atm) and 200mmHg (0.263atm) [24]. The gas sensing measurements of the CeO_2-based thick films presented a dual (electric and optical) gas sensing behavior when doped

with lanthanum on exposure to a carbon monoxide atmosphere at temperatures above 350°C. This was attributed to the itinerant 4f electrons created after the oxygen vacancy generation. Therefore, the precise role of oxygen vacancies is crucial to develop improved understanding of this important oxide material. However, creating these favorable defects and understanding their roles in the atomic level activity of nanosized CeO_2 is still lacking. Thus, there is a need to study the vacancy structure of these oxides using a probe that can provide information at the atomic level.

The most important properties found on doping CeO_2 with La was the rapid change in the electrical and optical responses in comparison with the pure CeO_2, only presenting electrical changes. Once the gas sensing measurements of the 8wt% La-doped CeO_2 sample depicted a peculiar dual-sensing behavior [20], not seen in the pure, 4wt% and 12wt% systems, we have focused our attention on this particular system, to specifically study the dependence of rare-earth modification with an AC bias (V) application under vacuum and air (~20% O_2) exposure, differing from the classical Schottky-type semiconductors, to determine the most likely conduction mechanism for nanostructured CeO_2-based systems.

Once the core electrons retain their atomic character, even when atoms form a solid, the experimental results can be directly compared to the theoretical predictions obtained by density functional theory (DFT). Therefore, a mixed theoretical-experimental approach was used to fully comprehend the dependence of rare-earth modification, with its dual behavior, in an AC bias (V) application under vacuum and air (~20% O_2) exposure to determine the most likely conduction mechanism for nanostructured CeO_2-based systems, in terms of capacitance variation, in accordance with the hopping conduction mechanism, differing from classical Schottky-type semiconductors, combined with *ab initio* studies.

2. Experimental Section

2.1 Nanomaterials preparation and characterization

The complete description regarding the nanopowder preparation by the microwave-assisted hydrothermal (MAH) method as well as the film fabrication via a hand-made simple deposition is thoroughly and precisely reported in several works [25–27].

CIS of the films was performed using an HP4284A impedance analyzer in a closed "device for the optoelectronic characterization of materials", under patent in Brazil (BR102016028383) and Argentina (AR103692). The measurements were made at 200 and 400°C, owing to the color change phenomenon occurring in the 8wt% La-doped CeO_2 sample [25]. Atmosphere changes were conducted with three different oxygen partial pressures (pO_2) from vacuum (10^{-3} mmHg or $1.33x10^{-6}$ bar) to 10mmHg (0.013 atm) and 50mmHg (0.065 atm) of synthetic air (20% O_2). For the atmosphere exposure analysis, an applied magnitude of excitation current of 1mA was used with the two-point probe technique in an AC-type measurement on a frequency interval of 10 Hz - 1 MHz.

It is worth mentioning that owing to the applied current range, the samples present an Ohmic behavior, and the electrodes capacitance contribution can be ignored. To ensure that the electric response was exclusively generated by the exposure to the different atmospheres, the films were thermally treated thrice (3x) in a closed atmosphere of dry synthetic air up to 380°C with a 1K/min rate and kept for 2h. Therefore, no traces of humidity or even glycerol (boiling point at 760mmHg: 563 K [28]) influenced the measurements.

2.2 Theoretical Approach and Computational Details

Our *ab initio* investigations are based on DFT [29,30] calculations employing the semi-local Perdew-Burke-Ernzerhof [31] exchange and correlation energy functional within the spin-polarized generalized gradient approximation (GGA) formulation. The Kohn-Sham equations were solved by using the all-electron projector augmented plane wave (PAW) method [32,33], which employed the following projectors $Ce(4f^1, 5d^1, 6s^2)$, $O(2s^2, 2p^4)$, and $La(5d^1, 6s^2)$, where the valence states are shown in the parenthesis. The calculations were performed with the Viena a*b initio* simulation package (VASP) [34,35] - version 5.4.4. The equilibrium volume of the CeO_2 unit-cell was reached by the minimization of the stress tensor by employing a plane wave basis with a kinetic energy cut-off of 829 eV. In addition, for the atomic forces optimizations, a plane wave basis with a cut-off of 466 eV was used, which was 12.5% higher than the value recommended

by the VASP package. A k-mesh of 2x2x2 was used to integrate the Brillouin zone for the stress tensor and atomic force optimizations, and twice for the electronic properties. A Gaussian smearing of 0.01eV was employed in all the calculations, and the atoms were allowed to relax until all the forces were smaller than 0.01eV/A on each atom. To obtain a better description of the large CeO_2 energy gap and band structure, we adopted the Hubbard correction (GGA+U) method [36], where U parameters are 4.50 eV, 5.0 eV and 5.50 eV on f-La, f-Ce, and p-O states, respectively, in accordance with literature [33,34].

3. Results and Discussions

3.1 Complex Impedance Spectroscopy (CIS)

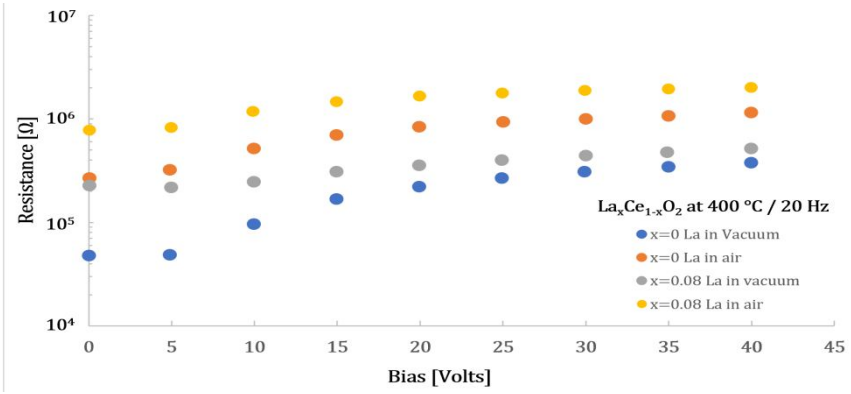

Figure 2 – Resistance x Bias(V) for pure and doped samples in vacuum and air atmospheres. Consider the air atmosphere with a 50mmHg of oxygen partial pressure (pO_2).

The resistance x bias (V) dependence for the pure and La-doped films can be seen in Figure 2, depicting the effect of the lanthanum addition on the electrical resistance of the films with a lower valence state of La^{3+} (r = 0.110 nm) than Ce^{4+} (r = 0.097 nm) at distinct applied voltages. A mild dependence of resistance (Ω) x bias (V) can be observed at Figure 2, and it is related to the voltage coefficient of resistance (VCR), expressed as the ratio of the resistance change in ohms to the corresponding increase in the applied voltage, in Volts, when the temperature is constant. Most resistors have a negative VCR [39], which implies that at high voltages, the resistance decreases during the pulse. However, a reduction in the electrical

conductivity is observed for both vacuum and air atmospheres in the entire range along with a structural expansion after lanthanum addition [23]. This indicates that our samples present a positive resistance coefficient, with a remarkable dependence for the pure CeO_2 film, increasing its resistance for the high-voltage regime. The modification with La decreased the positive VCR behavior, which depends not only on the length of the resistor but also on the conductive interfaces between the particles, which can lead to emission of charge carriers across particles gaps, via hopping conduction.

Additionally, the modification with lanthanum increases the electrical resistance in the entire voltage range, although the VCR decreases. This behavior can be interpreted as a consequence of the decrease in the number of Ce(III) species on the film surface. Details regarding the intermediate and high-voltage regimes are found to depend strongly on the doping density and energy distribution of the defect states, because the current-voltage non-linearities found in real materials are most probably associated with the defect state densities, which decrease above zero bias [40]. In fact, doping CeO_2 with lanthanum generates more ionized oxygen vacancies. Once CeO_2-based films present hopping electrons localized at the 4f states, corresponding to Ce(III) species, La^{3+} doping changes the oxidation of the Ce(III) species to Ce(IV), shifting down the Fermi level. Thus, few electrons in the 4f states are available for electrical conduction, thereby increasing its total electrical resistance.

In previous works, structural evidences have been used to deduce that the distribution of La^{3+} in the CeO_2 structure is random [41], and in particular, that the formation of oxygen vacancies [42,43] is accompanied by a reduction of the Ce^{4+} to Ce^{3+} states. Following the findings of Heinmaa et al. [40] regarding oxygen anion migration, O'Neill and Morris [41] further supported the concept that oxygen anions are mobile and distributed randomly throughout the CeO_2 structure. Contrastingly, phenomena associated with oxidation from the Ce^{3+} to Ce^{4+} states

have been reported [44], because of the oxygen exchange between the ambient gas-phase oxygen and structural oxygen in the oxide. Indeed, this oxidation from Ce^{3+} to Ce^{4+}, along with an increase of 8% in the defective oxygen species, according to XPS analyses, was seen in our previous report (under review - APSUSC-D-19-13517), due to the modification with Lanthanum.

To study the gaseous adsorption phenomena and the induced changes in the carrier concentration, we analyzed the film grain boundary capacitances obtained at a frequency of 1MHz from the total parallel capacitance [45]. This study is shown in Figure 3. The non-overlapping barriers in semiconductors are related to changes in the grain boundary capacitance during bias-measurements when the conduction mechanism considers parabolic-type potential barriers on the grain surface (band bending). For the CeO_2 samples, we must consider that the hopping of electrons between 4f states is responsible for the electrical conduction along with the intermediate energy levels [46] because of the large 6eV band gap.

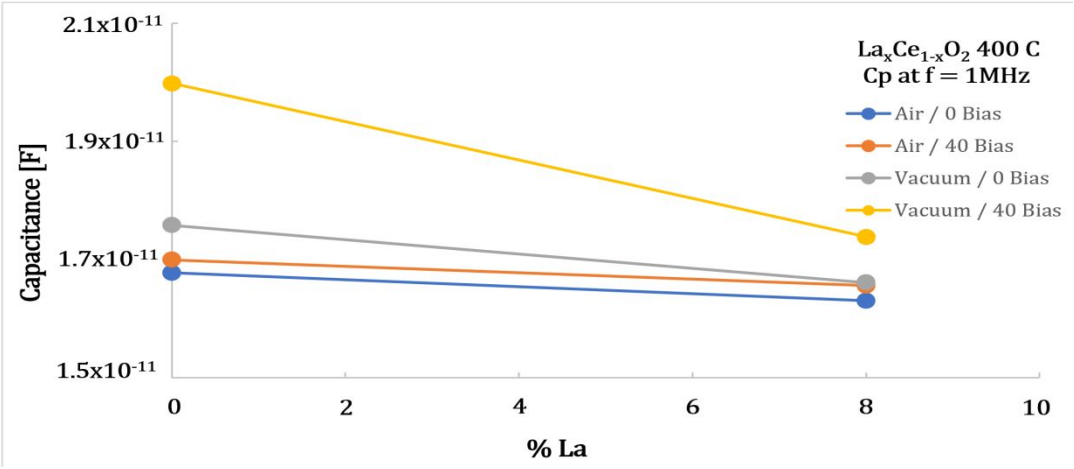

Figure 3 – Capacitance x %La for distinct applied voltages and atmospheres.

After exposure to air atmosphere, the capacitance (Cp) shows a slight decrease for increasing La-doped system. This can be interpreted as an exchange interaction between oxygen species in the air atmosphere with the CeO_2 structure, annihilating the oxygen vacancies. This process reduces the number of charge carriers, and thereby, the capability to store charges. After

the modification with lanthanum, the film capacitances in both the atmospheres and at the applied voltages were reduced, indicating a decrease in the density of the defective Ce(III) species that possess itinerant 4f electrons responsible for the electrical hopping conduction mechanism. This is a typical behavior presented in semiconductor oxides, where the number of defective species is decreased as the bias increases, in good agreement with previous works explaining the semiconductor oxide capacitance dependence on the applied voltages [47]. Worth to mention that the solid-lines used to connect the 0 and 8wt% points serve only as guides to give higher contrast in the figure, once the observed trends with distinct amounts of La do not present a linear behavior as shown in the following measurements.

In Figures 4 (a) and (b), pure and La-doped CeO_2 impedance plots are presented for 200 and 400°C in vacuum and oxygen-rich atmospheres. This is done to analyze the influence of the adsorbed oxygen species on the films surface and their diffusion into the grains along with the consequent annihilation of the oxygen vacancies and reduction in the donor concentration. The opposite phenomena occur when oxygen diffuses out of the grains, generating vacancies, as in the case of the interaction with $CO_{(g)}$. The relevant reactions for the oxygen species from the gas phase to the bulk of the grain are thoroughly reported elsewhere [46,48]. However, if the surface is treated with a reducing atmosphere, oxygen species migrates to the surface generating oxygen vacancies in an exchange process [44].

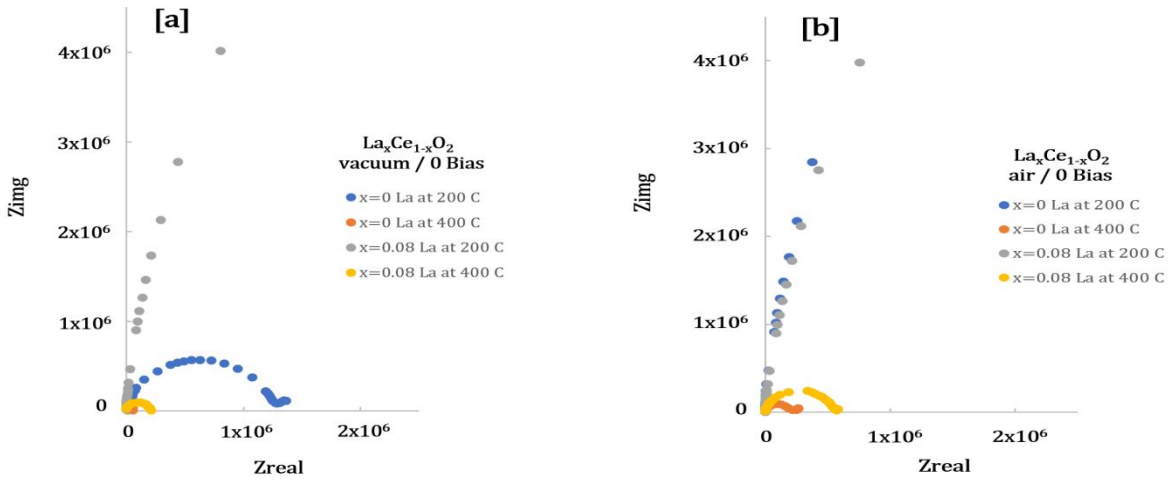

Figure 4 – Impedance plots for the pure and doped systems in (a) vacuum and (b) air at 0V for 200 and 400°C.

It can be seen that the conduction is thermally favored in both samples once the semicircle diameter is reduced at 400°C. The lanthanum-doped sample presents a larger impedance than the pure system in both temperatures, indicating a decrease in the number of 4f electrons available for conduction. The introduction of a trivalent lanthanum (La^{3+}) in the structure promotes the creation of a relatively higher number of oxygen vacancies along with a narrowing of the energy of the Fermi level and valence band (E_F-E_v). These two phenomena can induce opposite effects on the final electrical resistance of the samples, with the vacancy generation increasing the number of electrons in the 4f states along with the conductivity. Contrastingly, if the Fermi level (E_F) moves down, then E_{4f}-E_F increases and sample conductivity decreases. These phenomena were also observed in a previous work where a europium-doped CeO_2 sample presented a slightly small band gap value of 3.26eV, becoming less conductive compared to the pure sample [26].

By comparing Figures 4 (a) and (b), we can deduce the interaction of oxygen with the grain surfaces, which finally reduces the number of $4f^1$ electrons. A large impedance increase is observed for pure and doped samples exposed to air atmospheres at 200 and 400°C, when compared to the vacuum atmosphere. The oxygen interaction with the surface causes a transfer of electrons from the bulk ($4f^1$ states), which also modifies the energy difference between the Fermi level and 4f state at the band gap (E_{4f}-E_F). The density of the carriers decreases and, consequently, the sample impedance increases with doping, in both temperature regimes. Hence, the introduction of lanthanum in the structure imposes a narrowing effect on the energy gap (E_F – E_v), causing an increase in the sample resistivity because of the relatively larger number of bulk Ce(IV) species with no 4f electrons available for conduction.

The capacitance dependence on the frequency for the pure and doped samples in vacuum and air atmospheres at 200 and 400°C can be seen in Figures 5 (a) and (b).

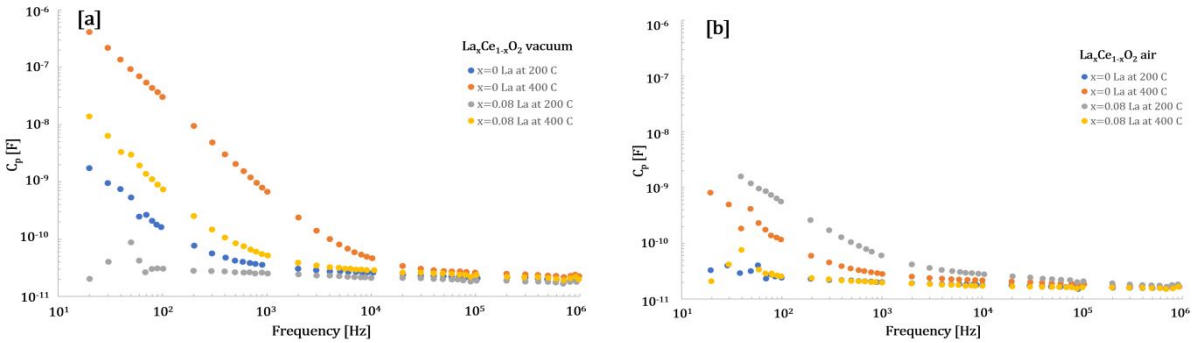

Figure 5 – Capacitance (Cp) x frequency (Hz) in (a) vacuum and (b) air atmospheres.

The observed behavior suggests the possible presence of multi-traps, which depends on the described equilibrium between the oxygen vacancies ($V_o^x \longleftrightarrow V_O^{\cdot} \longleftrightarrow V_O^{\cdot\cdot}$) in the CeO_2 samples with a $1/f^2$(Hz) dependence of Cp. The latter shows an inflection point corresponding to a critical frequency, named "corner frequency" [46], with a disordered deep bulk trap location. The multi-traps are considered responsible for the phenomenon that modifies the Debye-like response. When dealing with a distribution of activation energies and not a single activation energy, one shifts from a simple ideal resistor and capacitor in parallel case to a distribution of impedance elements (constant-phase element, CPE). Deep traps are activated with temperature as shown by the dependence of the square of the frequency for the samples exposed to vacuum and air atmospheres. Contrarily, the modification with lanthanum decreases the effect of the deep and shallow traps with frequency. Additionally, at the high frequencies, virtually no dependence of the capacitance on frequency at 200 and 400°C can be seen for both samples. Indeed, for the higher values, the sample capacitances have a mild dependence on the frequency. This behavior is consistent with the absence of band bending or with the band bending not affecting the sample capacitance. Deep bulk traps are affected by the doping, temperature, and atmosphere exposure, as shown in Figures 5 (a) and (b). When the samples are exposed to an air atmosphere, a decrease in the deep bulk traps distribution is observed at low frequencies. This can be probably

ascribed to traps deactivation because the samples are exposed to air owing to the slight shift of the Fermi level to relatively lower positions due to exchange interactions with the oxygen species [44].

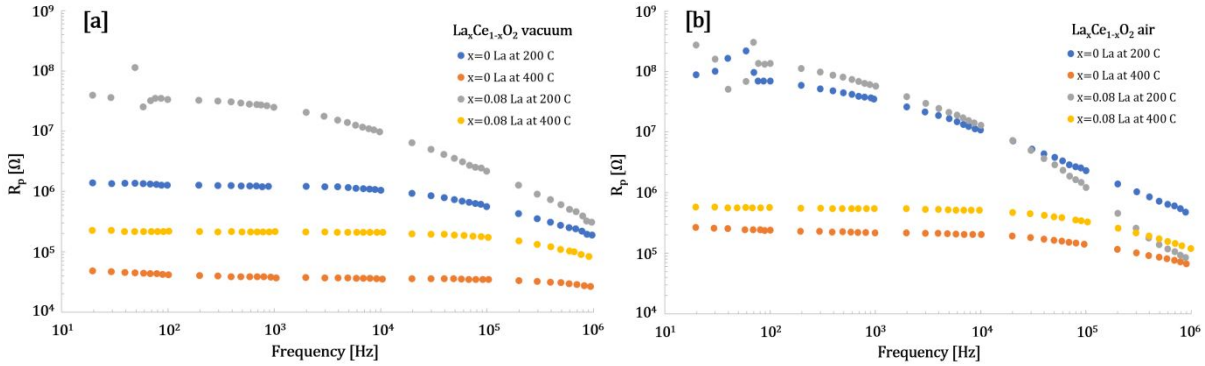

Figure 6 – Resistance (Rp) x frequency (Hz) in (a) vacuum and (b) air atmosphere.

The drop in the resistance with temperature, as seen in Figure 6, can be associated with the modification of the carrier transport because all transport mechanisms are facilitated with temperature. Under the experimental conditions in which the sample is exposed to vacuum and temperature is altered, a variation in the barrier height or width would not be possible. Therefore, the electronic hopping transport mechanism must be responsible for the observed changes in the resistance. These results are consistent with previous reports for polycrystalline semiconductors [48]. The observed Fermi level energy decrease, with lanthanum modification, increases the film resistance, as previously observed.

A mild dependence of the resistance with frequency is shown mostly at 200°C by both the pure and doped samples at frequencies higher than 10KHz. This indicates a behavior that cannot be appropriately described by a simple RC equivalent circuit, and therefore, probably needing an electrical circuit representation including the presence of multi-traps [41] corroborating the presence of defective oxygen species, such as vacancies. Therefore, we show that the frequency dependence of the total resistance and capacitance can be assigned to the presence of deep bulk traps, which are probably ascribed to the interactions of the defective oxygen and metallic species throughout the system.

As the antimatter equivalent of an electron, a positron is an extremely non-destructive sensitive probe of both the structural and electronic properties of solids. Among the different experimental variants of the positron annihilation spectroscopy (PAS), positron annihilation lifetime spectroscopy (PALS) has demonstrated to be the most adequate technique to study vacancy-like defects, providing quantitative sensitivity and selectivity to this type of defects [45]. Recently, several researchers used PALS to study the defect structure in different CeO_2-based nanostructured systems [46–49]. In particular, Xiangwen *et al*. [46] studied the influence of the defect structure on the catalytic activity of two CeO_2 nanorod samples synthesized using different methods. Moreover, Wang *et al*. [47] reported results on the role of oxygen vacancies in the catalytic performance for o-xylene oxidation of CeO_2 nanocubes calcinated at different temperatures. In both the cases, the authors reported the formation of small neutral Ce^{3+}-V_O associations, defined as $[Ce'_{Ce}\text{-}V_O^{\cdot\cdot}\text{-}Ce'_{Ce}]^x$, and large oxygen vacancy clusters. By contrast, Sachdeva et al. [48] studied the defect structure in $Ce_{1-x}Nd_xO_{2-x/2}$ nanostructured samples with x ranging from 0.076 to 0.675. For nominal Nd concentrations lower than 0.4, the authors proposed the formation of neutral Nd-oxygen vacancy clusters defined as $[Nd'_{Ce}\text{-}V_O^{\cdot\cdot}\text{-}Nd'_{Ce}]^x$. Similarly, Thorat et al. [49] reported a systematic study of the defects generated in samples of nanostructured CeO_2 samples doped with different concentrations of Eu ranging from 0 to 50 atom%. In this work, the authors reported that for Eu concentrations lower than 1%, the dominant defects were Ce^{3+}-V_O-type associates. At relatively higher Eu concentrations, these associates agglomerated to form larger V_O clusters including Ce^{3+} and Eu^{3+} species. Furthermore, the preliminary PALS results measuring the nanostructured pure and lanthanum-

doped CeO_2 samples indicated that the defect structures of these samples were consistent with the existence of the vacancy-like associates described hereafter.

To understand the interaction between the vacancy-defects and metal species, we must first consider the resonant equilibrium between the ordered and disordered $[CeO_8]$ clusters, represented as:

$$[CeO_8]^{x}_{o} \leftrightarrow [CeO_8]^{x}_{d} \quad (1)$$

Then, we can consider the intrinsic generation of oxygen vacancies such as

$$[MO_8]^{x}_{o} + [MO_8]^{x}_{d} \rightarrow [MO_8]'_{o} + [MO_7.V^{\cdot}_{o}] + \tfrac{1}{2} O_2 \quad (2)$$

$$[MO_8]^{x}_{o} + [MO_7.V^{\cdot}_{o}] \rightarrow [MO_8]'_{o} + [MO_7.V^{\cdot\cdot}_{o}] \quad (3)$$

$$[MO_8]^{x}_{o} + [MO_7.V^{x}_{o}] \rightarrow [MO_8]'_{o} + [MO_7.V^{\cdot}_{o}] \quad (4)$$

$$[MO_7.V^{x}_{O}] + [MO_7.V^{\cdot}_{O}] \rightarrow [MO_7.V^{x}_{O}]^{'}_{o} + [MO_7.V^{\cdot\cdot}_{O}] \quad (5)$$

where M represents a rare-earth element. The a*b initio* studies indicate that under oxygen-poor conditions, the defects with the lowest formation energy are oxygen vacancies, whereas oxygen interstitials, which form peroxide ions, will be more favorable under oxygen-rich conditions, with oxygen vacancies typically being the dominant defect [38]. Additionally, the interaction of an oxygen vacancy with one or two substitutional elements will depend on the radius size of the dopant, with a first-neighbor interaction occurring for small elements and a second-neighbor interaction occurring with large dopants. Once the experimental measurements were performed with an oxygen partial pressure (pO_2) up to 0.065atm and that an air atmosphere

can be considered when pO_2 = 0.2atm, we can admit our experimental parameters as under oxygen-poor conditions with oxygen vacancies being the most likely defects.

In air atmosphere, the interaction of oxygen species with these clusters can be probably considered as:

$$[MO_7.V_o^z] + O_2 \rightarrow [MO_7.V_o^z]...O_{2(ads)}, \text{ where } V_o^z = V_o^x, V_o^{\cdot} \text{ or } V_o^{\cdot\cdot} \quad (6)$$

$$[MO_7.V_o^x]...O_2 \rightarrow [MO_7.V_o^{\cdot}]...O'_{2(ads)} \quad (7)$$

$$[MO_7.V_o^{\cdot\cdot}] + O_2 \rightarrow [MO_7.V_o^{\cdot\cdot}]...O_{2(ads)} \quad (8)$$

We must also consider that different oxygen species can be formed depending on the working temperature [50]. For CeO_2 clusters, we can rewrite equations 6 and 7 as:

$$[CeO_7.V_o^x]...O_{2(ads)} \rightarrow [CeO_7.V_o^{\bullet}]...O_2'(ads) \quad (9)$$

$$[CeO_7.V_o^{\cdot}]...O_2 \rightarrow [CeO_7.V_o^{\cdot}]...O'_{2(ads)}, \text{ for } T > 573K \quad (10)$$

The ionized oxygen species adsorbed on the CeO_2 surface can also be represented by equations 9 and 10. We can also consider the transfer of an electron from Ce(III) to the oxygen species, decreasing the number of electrons in the 4f states and reducing the electrical conductivity by hopping. This occurs according to the following steps, which differ depending on the ceria cluster interacting directly with the oxygen molecules in the atmosphere. In this case, the presence of $Ce_{Ce}^{'}$-type species, which represent the presence of Ce(III) can be considered as polarons, which likely contribute to the electrical conduction mechanism [51].

18

$$[CeO_{7}.V_{o}^{x}]...O_{2\,(ads)} + [CeO_{8}]_{o}' \rightarrow [CeO_{7}.V_{o}^{x}]...O_{2}' + [CeO_{8}]_{o}^{x} \quad (11)$$

$$[CeO_{7}.V_{o}^{\bullet}]...O_{2(ads)} + [CeO_{8}]_{o}' \rightarrow [CeO_{7}.V_{o}^{\bullet}]...O_{2}' + [CeO_{8}]_{o}^{x} \quad (12)$$

$$[CeO_{7}.V_{o}^{\bullet\bullet}]...O_{2(ads)} + [CeO_{8}]_{o}' \rightarrow [CeO_{7}.V_{o}^{\bullet\bullet}]...O_{2}' + [CeO_{8}]_{o}^{x} \quad (13)$$

$$[CeO_{7}.V_{o}^{x}] + [CeO_{7}.V_{o}^{\bullet}]\ldots O_{2} \rightarrow [CeO_{7}.V_{o}^{\bullet}]\ldots O_{2}' + [CeO_{7}.V_{o}^{\bullet}] \quad (14)$$

For the lanthanum-doped sample, we must also consider the presence of lanthanum complex clusters, represented as follows:

$$[LaO_{8}]_{o}^{x} + [LaO_{7}.V_{O}^{x}] \rightarrow [LaO_{8}]_{o}' + [LaO_{7}.V_{O}^{\cdot}] \quad (15)$$

$$[LaO_{8}]_{o}^{x} \ldots [LaO_{7}.V_{O}^{x}] \rightarrow [LaO_{8}]_{o}' \ldots [LaO_{7}.V_{O}^{\cdot}] \quad (16)$$

$$[CeO_{8}]_{o}^{x} \ldots [LaO_{7}.V_{O}^{x}] \rightarrow [CeO_{8}]_{o}^{'} \ldots [LaO_{7}.V_{O}^{\cdot}] \quad (17)$$

$$[CeO_{8}]_{o}' + [LaO_{7}.V_{o}^{\bullet}] \rightarrow [CeO_{7.}V_{o}^{\bullet}] + [LaO_{8}.]_{o}' \quad (18)$$

We can also consider a doubly-ionized oxygen vacancy formation that does not lead to an electrical resistance change, although it can correspond to an excellent positron trapping site. This doubly-ionized oxygen vacancy formation can be expressed as.

19

$$[LaO_8]_o^x ...[CeO_7 . V_o^x]\ldots[LaO_8]_o^x \leftrightarrow [LaO_8]_o' ...[CeO_7 . V_o^{..}] ... [LaO_8]_o' \quad (19)$$

Additionally, the contribution of the oxidation state fluctuation for the lanthanum atoms should be considered, as represented in the equation below. It can also lead to a positron trapping site but do not increase the sample resistance.

$$[LaO_8]_o' \ldots[CeO_7 . V_o^{\bullet}]\ldots [LaO_8]_o^x \rightarrow [LaO_8]_o' ...[CeO_7 . V_o^{\bullet\bullet}]... [LaO_8]_o' \quad (20)$$

The following equation represents the increase in paramagnetic species, when the samples are doped, along with an increase in the number of defective clusters and decrease in Ce^{3+} species, as previously referenced. This equation is confirmed in the experimental measurements and theoretical investigation.

$$[CeO_8]_o^{,} + 2[LaO_8]^x + [CeO_7 . V_o^x] \leftrightarrow [CeO_8]_o^x + [LaO_8]_o^{,} ...[CeO_7 . V_o^{.}]\ldots [LaO_8]_o^{,} \quad (21)$$

3.2 *Ab initio* studies

The use of ab initio calculations allows getting a precise microscopic scenario of electronic levels distribution of pure and rare-earth-doped Ceria. Žguns and co-workers found that for Gd-doped CeO_2, there exists a transition temperature (T_c) below which phase separation into C-type Gd_2O_3 and pure CeO_2 occurs. In the thermodynamic equilibrium, they observed two transitions: the onset of oxygen-vacancy (O–Va) ordering at ca. 1200–3300 K for concentrations x_{Gd} = 0.3–1, and a phase separation into CeO_2 and C-type Gd_2O_3 occurring below ca. 1000 K

for all concentrations. They also modeled 'quenched' systems, with cations immobile below 1500 K, and observed that the presence of random-like cation configurations did not prevent C-type vacancy ordering [57]. The phase separation was observed in the whole studied concentration range (x < 25%wt Gd) and the transition temperature increased with concentration from ca. 600 (x_{Gd} = 0.03) to 1000 K (x_{Gd} = 0.25). Above T_c the distribution of Gd is random, with oxygen vacancies clustering in the coordination shells along 〈1, 1/2, 0〉 and 〈1, 1, 1〉, and the nearest neighbor position being preferred for Gd-vacancy [58]Koettgen and coworkers pointed out that the ionic conductivity is influenced by trapping, blocking and vacancy–vacancy interactions [59–61]. The blocking mechanism mainly limits the dopant fraction at the ionic conductivity, and is generally strongly underrated in the literature. Trapping mainly limits the maximum ionic conductivity value, with the association energy differences being decisive. The trapping predominantly influences the maximum ionic conductivity as well as the apparent activation enthalpy. The highest conductivity can be found if all absolute values of the association energy differences are small. The rare-earth-vacancy (RE–V) association leads to the formation of associates, i.e. vacancies are held by the dopants as their movement is hindered. The long-range RE–V association catches vacancies into the vicinity of dopants. Both catch-and-hold need to be small for a large ionic conductivity. The catch-and-hold principle easily predicts the dopant that leads to the highest ionic conductivity [60].

According to our investigations, the calculated lattice parameter by using the Hubbard model for the CeO_2 pristine cubic unit-cell, with space group Fm-3m, is 5.47Å, whereas the experimental value is 5.41Å, a deviation of only 0.06Å. To avoid the interaction between neighboring images, our calculations were performed by using a CeO_2 supercell extended in two of the three Cartesian directions, with one lanthanum atom replacing one cerium in the bulk. There are 63 O (red) , 31 Ce (purple) and 1 La (black) atoms, corresponding to a 3.2% of La-impurity concentration, and the structure has an oxygen vacancy, as depicted in Figure 7. The oxygen vacancies are placed near (left panel) and far (right panel) from the lanthanum atom in the bulk. In the pristine supercell, each cerium atom is surrounded by eight oxygen atoms. Aiming to investigate the localized magnetic moments, we calculated the spin charge density,

$\Delta\rho=\rho\uparrow-\rho\downarrow$, by using an isosurface of +0.007 e/Å^3, as depicted in the same panel. In these calculations, a strong localized magnetic moment appears on one cerium atom of the supercell, which varies the oxidation state of cerium and is responsible for the consequent generation of defective clusters that improve the electrical response and likely creates the optical emission phenomena when exposed to a CO atmosphere. The position of this localized magnetic moment depends on the oxygen vacancy position, as shown in Figure 7. The localized magnetic moment on the cerium atom indicates the presence of Ce^{+3} and oxygen vacancies, which varies the conductivity of the material in agreement with our experimental results. In these calculations, we observe that the presence and position of the oxygen vacancy are crucial to determine the localized magnetic moment on a specific cerium atom. Thus, for a proximal (distant) oxygen vacancy from the lanthanum atom, the localized magnetic moment appears far (near) from the vacancy, as shown in Figure 6. Similarly, the study of defects is a dominating factor for the symmetry of the geometry, which can modify the magnetic ordering of the supercell atoms.

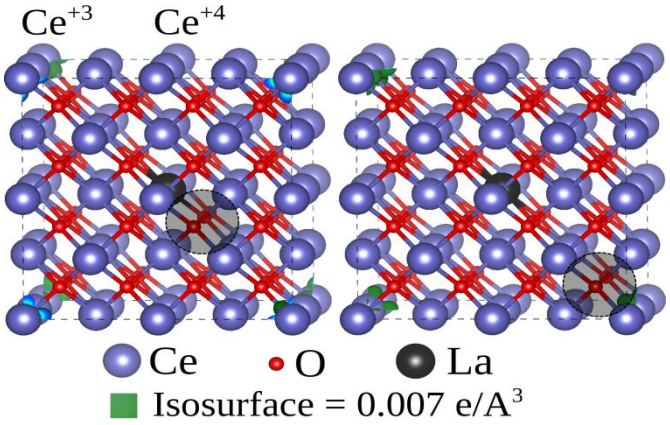

Figure 7 - Calculated bulk structures for a lanthanum-doped cerium oxide with one oxygen vacancy.

In addition, the electronic properties were investigated by using the calculated density of states per atom, as depicted in Figure 8, for the previously presented structures. In Figure 8, the left (right) panel depicts CeO_2 doped by lanthanum atom with one oxygen vacancy near (far) from the impurity. It is worth mentioning that the consideration of an oxygen deficiency far from the lanthanum atom, corresponding to the experimental behavior of a more resistive sample, can

22

be represented by equation 18, where the Ce^{3+} specimen is depicted by $[CeO_8]^{\prime\prime}_o$. In fact, when we think of nanostructured CeO_2-based systems, the tiniest change of the first-neighboring atoms would create distinct dipole moments with differing electronic densities (eg. Ce(III)-Ce(III), Ce(III)-Ce(IV), Ce(III)-La(III), and Ce(IV)-La(III)), not to mention rare-earth-vacancy (RE-V) interactions. Besides, one can also consider the break of local symmetry which has direct consequences on the electrical band-gap, leading to distinct density of states as shown in Figure 8.

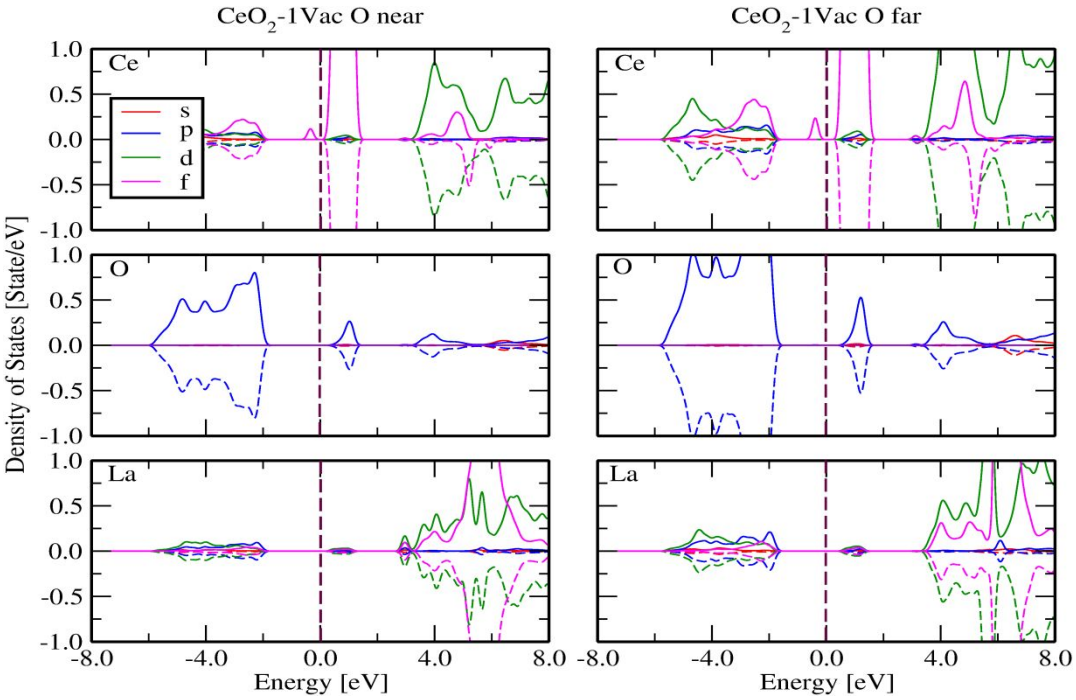

Figure 8 - Density of states of cerium oxide doped by a lanthanum impurity with an oxygen deficiency near (left panel) and far (right panel) from the lanthanum. The Fermi energy is taken as 0.0 eV.

For both structures, the dominant contributions for the occupied electronic states are given by p-La, p-O and f-Ce, while the major contributions for unoccupied states are d-La, f-La, p-O, d-Ce and f-Ce. Note that, in the cerium density of states, the isolated f-Ce spin-up state depicts the localized magnetic moments of Ce+3 atoms, as depicted in Fig. 7. Thus, the occupied

f-Ce electronic states near the Fermi energy is in agreement with the presence of 4f-electrons proposed as the hopping electrical conduction mechanism for the samples.

According to the experimental results given in section 3.1, after modification with lanthanum, the sample becomes more resistive in both the vacuum and air atmospheres, being a good indicator that the electrons from the Ce $4f^1$ states decay to the La f-states (showed in Figure 8-DOS). Additionally, *ab initio* calculations are strictly related to equations (1)-(20), helping to understand the weight of each path in the transport properties of pure and La-doped CeO2, with electrons injected in the structure by defect equilibria having the possibility to spend their time on Ce, La or oxygen vacancies. Having a look to Figure 8, one can see that the Ce-DoS around 1eV are much larger than La ones, therefore we can conclude that most of the time, the electrons are likely to stay in $[Ce^{3+}]>>[La^{3+}]$.

In this way, our system is predominantly composed of oxygen vacancies near the lanthanum atoms, whose f-level energies are shifted from the Fermi level, in good agreement with the previous results reported by *Skorodumova et. al*. [52], Deduchi *et. al.* [53], and Yoshida *et. al.* [54]. In addition, according to the electrical transport defined by the cluster-to-cluster charge transfer (CCCT) [54], the probability of a hopping/tunneling transition is determined by the distance between the available sites and potential barrier to be overcome. If the distance is longer than 10Å, then an electron would hop rather than tunnel [55]. Therefore, considering the unit cell given in Figure 7 with an experimental lattice parameter (*a*) of approximately 5Å, the electrical transport within the structure and along the first neighbors would be predominantly composed of tunneling electrons along defective Ce(III) species, whereas the transfer of electrons throughout the bulk would be virtually formed of hopping processes.

4. CONCLUSIONS

The combination of experimental and theoretical approaches to understand the electrical behavior of our CeO_2-based samples revealed that the hopping/tunneling of electrons in the 4f states must be considered being the responsible mechanism of the CCCT electrical conduction, along with the lanthanum intermediate-energy f-states. The presence of multi-traps was confirmed, which depended on the described equilibrium between the oxygen vacancies ($V_o^x \longleftrightarrow V_O^{\cdot} \longleftrightarrow V_O^{\cdot\cdot}$) as well as on their interaction in the distinct defective clusters with available electronic density for conduction. The modification with lanthanum increased the electrical resistance of the system, although the voltage coefficient of resistance (VCR) decreased, which was interpreted as a consequence of the decrease in the number of Ce(III) species. This was a good indicator that electrons from Ce $4f^1$ states decayed to La f-states. Indeed, doping CeO_2 with lanthanum generated more ionized oxygen vacancies close to the lanthanum atoms. The new formed La f-states induced the Ce(III) species to undergo oxidation to Ce(IV) owing to the Fermi level shifting. Thus, relatively fewer electrons in the 4f states were available for electrical conduction, increasing its total electrical resistance. The film capacitance in both the atmospheres and at the applied voltages was reduced, indicating a decrease in the density of the defective Ce(III) species possessing itinerant 4f electrons responsible for the electrical conduction mechanism. Therefore, we showed that the frequency dependence of the total resistance and capacitance could be associated with the presence of deep bulk traps (polarons), which in turn were ascribed to the interactions of the defective oxygen and rare-earth species throughout the system, corroborating the cluster-to-cluster charge transfer (CCCT) mechanism. Additionally, according to the theoretical investigations, our system was predominantly conformed of oxygen vacancies located near from the lanthanum atoms, whose f-level energies shifted from the Fermi level. Furthermore, according to the electrical transport defined by the CCCT probability of the hopping transition, and consideration of a the unit cell

with an experimental lattice parameter (a) of approximately 5Å, the electrical transport within the unit cell and along the first neighbors would be predominantly composed of tunneling electrons. By contrast, the transfer of electrons throughout the bulk would be virtually formed of hopping processes with the oxygen vacancies playing the major role in the conductivity of the ceria-based materials.

Corresponding Author

*leandro.rocha@liec.ufscar.br

Author Contributions

The manuscript was written through contributions of all authors. All authors have given approval to the final version of the manuscript.

Funding Sources

CAPES, CNPq, FAPESP.

ACKNOWLEDGMENT

The authors thank the following Brazilian agencies for their financial support of this research project: "*Coordenação de Aperfeiçoamento de Pessoal de Nível Superior"* - Brazil (CAPES) - Finance Code 001, the National Council for Scientific and Technological Development (CNPq), and "*Fundação de Amparo à Pesquisa do Estado de São Paulo"* (FAPESP), grants n° 2013/07296-2 (CEPID), 2014/19142-2, 2016/25500-4, 2017/19143-7, 2018/20729-9 and 2018/20590-0.

REFERENCES

1. Wang L-S; Li C-X; Li C-J; Yang G-J. Performance Of $La_{0.8}Sr_{0.2}Ga_{0.8}Mg_{0.2}O_3$-Based SOFCs With Atmospheric Plasma Sprayed La-Doped CeO_2 Buffer Layer. *Electrochim Acta* **2018** 275:208–217

2. Hussain S; Aslam N; Yang Xy; Javed, M. S.; Xu, Z.; Wang, M.; Liu, G.; Qiao, G. Unique Polyhedron CeO_2 Nanostructures For Superior Formaldehyde Gas-Sensing Performances. *Ceram Int* **2018** 44:19624–19630

3. Singh K; Kumar K; Srivastava S; Chowdhury A; Effect Of Rare-Earth Doping In CeO_2 Matrix: Correlations With Structure, Catalytic And Visible Light Photocatalytic Properties *Ceram Int* **2017** 43:17041–17047

4. Chen, M.; Gao, H.; Zhang, L.; Xuan, Y.; Ren, J.; Ni, M.; Lin, Z. Unlocking The Nature Of The Co-Doping Effect On The Ionic Conductivity Of CeO_2-Based Electrolyte. *Ceram Int* **2019** 45:3977–3985

5. Nagaraju, P.; Vijayakumar, Y.; Radhika, P.; Choudhary, R.J.; RamanaReddy, M.V. Structural, Morphological, Optical And Gas Sensing Properties Of Nanocrystalline Ceria Thin Films. *Mater Today Proc* **2016** 3:4009–4018

6. Marabelli, F.; Wachter, P. Covalent Insulator CeO_2: Optical Reflectivity Measurements. *Phys Rev B* **1987** 36:1238–1243

7. Tiwari, S.; Rathore, G.; Patra, N.; Yadav, A.K.; Bhattacharya, D.; Jha, S.N.; Tseng, C.M.; Liu, S. W.; Biring, S.; Sen, S. Oxygen And Cerium Defects Mediated Changes In Structural, Optical And Photoluminescence Properties Of Ni Substituted CeO_2. *J Alloys Compd*. **2019** 782:689–698

8. Mittal, M.; Gupta, A.; Pandey, Op. Role Of Oxygen Vacancies In Ag/Au Doped CeO_2 Nanoparticles For Fast Photocatalysis. *Sol Energy* **2018** 165:206–216

9. Sun, Q.; Fu, Z.; Yang, Z. Effects Of Rare-Earth Doping On The Ionic Conduction Of CeO_2 In Solid Oxide Fuel Cells. *Ceram Int* **2018** 44:3707–3711

10. Esch, F.; Fabris, S.; Zhou, L.; Montini, T.; Africh, C.; Fornasiero, P.; Comelli, G.; Rosei, R. Electron Localization Determines Defect Formation On Ceria Substrates. *Science* **2005** 309(5735):752-755

11. Tuller, H.L.; Nowick A.S. Small Polaron Electron Transport In Reduced CeO_2 Single Crystals. *J Phys Chem Solids* **1977** 38:859–867

12. Rao, G.V.S.; Ramdas S.; Mehrotra P.N.; Rao C.N.R. Electrical Transport In Rare-Earth Oxides. *J Solid State Chem* **1970** 2:377–384

13. Huang, S.; Li, L.; Van Der Biest, O.; Vleugels, J. Influence Of The Oxygen Partial Pressure On The Reduction Of CeO_2 And CeO_2ZrO_2 Ceramics. *Solid State Sci* **2005** 7:539–544

14. Blumenthal, R.N.; Hofmaier, R.L. The Temperature And Compositional Dependence Of The Electrical Conductivity Of Nonstoichiometric CeO_{2-X}. *J Electrochem Soc* **1974** 121:126

15. Blumenthal, R.N.; Sharma, R.K. Electronic Conductivity In Nonstoichiometric Cerium Dioxide. *J Solid State Chem* **1975** 13:360–364

16. Kullgren, J.; Castleton, C.W.M.; Müller, C.; Ramo, D.M.; Hermansson, K. B3lyp Calculations Of Cerium Oxides. *J. Chem. Phys.* **2010** 132:1–12.

17. Kotani, A.; Parlebas, J.C. Core Photoemission Theory Of Semiconducting Rare Earth Compounds. *J Phys* **1985** 46:77–82

18. Hitchcock P.B.; Lappert M.F.; Maron, L.; Protchenko, A.V. Lanthanum Does Form Stable Molecular Compounds In The +2 Oxidation State. *Angew Chemie* **2008** 47:1510–1513

19. Milberg, B.; Juan, A.; Irigoyen, B.; Redox Behavior Of A Low-Doped Pr-CeO_2(111) Surface. A DFT+U Study. *Appl Surf Sci* **2017** 401:206–217

20. Rocha, L.S.R.; Cilense, M.; Ponce, M.A.; Aldao, C.M.; Oliveira, L.L.; Longo, E.; Simões, A.Z. Novel Gas Sensor With Dual Response Under $CO_{(g)}$ Exposure: Optical And Electrical Stimuli. *Phys B Condens Matter* **2018** 536:280–288

21. Hong, S.J.; Virkar, A.V.; Lattice Parameters And Densities Of Rare-Earth Oxide Doped Ceria Electrolytes. *J Am Ceram Soc* **1995** 78:433–439

22. Ortega P.P.; Rocha L.S.R.; Cortés J.A.; Ramirez, M.A.; Buono, C.; Ponce, M.A.; Simões, A.Z. Towards Carbon Monoxide Sensors Based On Europium Doped Cerium Dioxide. *Appl Surf Sci* **2019** 464:692–699

23. Deus, R.C.; Amoresi R.A.C.; Desimone, P.M.; Schipani, F.; Rocha, L.S.R.; Ponce, M.A.; Simões, A.Z.; Longo, E. Electrical Behavior Of Cerium Dioxide Films Exposed To Different Gases Atmospheres. *Ceram Int* **2016** 42:15023–15029

24. Glycerin Producers' Association, *Physical Properties Of Glycerine And Its Solutions;* New York, 1963.

25. Hohenberg, P.; Kohn, W. Inhomogeneous Electron Gas. *Phys Rev* **1964** 136:B864–B871

26. Kohn, W.; Sham, L.J. Self-Consistent Equations Including Exchange And Correlation Effects. *Phys Rev* **1965** 140, A1133

27. Perdew, J.P.; Burke, K.; Ernzerhof, M. Generalized Gradient Approximation Made Simple. *Phys Rev Lett* **1996** 77:3865–3868

28. Blöchl, P.E. Projector Augmented-Wave Method. *Phys Rev B* **1994** 50:17953–17979

29. Kresse, G.; Joubert, D. From Ultrasoft Pseudopotentials To The Projector Augmented-Wave Method. *Phys Rev B* **1999** 59:1758–1775

30. Kresse, G.; Furthmüller, J. Efficient Iterative Schemes For Ab Initio Total-Energy Calculations Using A Plane-Wave Basis Set. *Phys Rev B* **1996** 54:11169–11186

31. J. Hafner, Materials simulations using VASP: a quantum perspective to materials science. *Comp. Chem. Comm.* **2007** 177:6-13

32. Alaydrus, M.; Sakaue, M.; Kasai, H. A DFT+U Study On The Contribution Of 4f Electrons To Oxygen Vacancy Formation And Migration In Ln-Doped CeO_2. *Phys Chem Chem Phys* **2016** 18:12938–12946

33. Chen, H.T. First-Principles Study Of Co Adsorption And Oxidation On Ru-Doped CeO_2(111) Surface. *J Phys Chem C* **2012** 116:6239–6246

34. Keating, P.R.L.; Scanlon D.O.; Morgan, B.J.; Galea, N.M.; Watson, G.W. Analysis Of Intrinsic Defects In CeO_2 Using A Koopmans-Like GGA+U Approach. *J Phys Chem C* **2012** 116:2443–2452

35. Boella, G.; Galliana, F. Analysis of the voltage coefficient of high value standard resistors. *Measurement* **2008** 41(1):1-9**.**

36. Pike, G.E.; Seager, C.H. The Dc Voltage Dependence Of Semiconductor Grain-Boundary Resistance. *J Appl Phys* **1979** 50:3414–3422

37. Heinmaa I.; Joon, T.; Kooskora, H.; Pahapill, J. Local Structure And Oxygen Ion Dynamics In La Doped Ceria: 17O NMR Study. *Solid State Ionics* **2010** 181:1309–1315

38. O'Neill, W.M.; Morris, M.A. The Defect Chemistry Of Lanthana–Ceria Mixed Oxides By MASNMR. *Chem Phys Lett* **1999** 305:389–394

39. Liu, L.; Wang, X.; Guo, M.; Zhang, M. Kinetics Investigation Of Oxygen Storage Capacity In La_2O_3–CeO_2 Solid Solution. *J Nanosci Nanotechnol* **2011** 11:2155–2162(8)

40. Ponce, M.A.; Castro M.S.; Aldao, C.M. Capacitance And Resistance Measurements Of SnO_2 Thick-Films. *J Mater Sci Mater Electron* **2009** 20:25–32

41. Deus, R.C.; Cortés J.A.; Ramirez, M.A.; Andrés, J.; Rocha, L.S.R.; Longo, E.; Simões, A.Z. Photoluminescence Properties Of Cerium Oxide Nanoparticles As A Function Of Lanthanum Content. *Mater Res Bull* **2015** 70:416–423

42. Ponce, M.A.; Castro M.S.; Aldao C.M. Influence Of Oxygen Adsorption And Diffusion On The Overlapping Of Intergranular Potential Barriers In SnO_2 Thick Films. *Mater Sci Eng B* **2004** 111:14–19

43. Li, C.; Domen, K.; Maruya, K.; Onishi, T. Oxygen Exchange Reactions Over Cerium Oxide: An FT-IR Study. *J Catal* **1990** 123:436–442

44. Keating, P.R.L.; Scanlon, D.O.; Watson, G.W. The Nature Of Oxygen States On The Surfaces Of CeO_2 And La-Doped CeO_2. *Chem Phys Lett* **2014** 608:239–243

45. Kirk, C.T. A Theory Of Transistor Cutoff Frequency (f_T) Falloff At High Current Densities. *Ire Trans Electron Devices* **1962** 9:164–174

46. Ponce, M.A.; Parra, R.; Savu R.; Joanni, E.; Bueno, P.R.; Cilense, M.; Varela, J.A.; Castro, M.S. Impedance Spectroscopy Analysis Of TiO_2 Thin Film Gas Sensors Obtained From Water-Based Anatase Colloids. *Sensors Actuators B Chem* **2009** 139:447–452

47. Chiou, B.S.; Chung, M.C. Admittance Spectroscopy And Trapping Phenomena Of ZnO Based Varistors. *J Electron Mater* **1991** 20:885–890

48. Hautojärvi, P.; Corbel, C. In *Positron Spectroscopy Of Defects In Metals And Semiconductors;* Dupasquier, A., Mills Jr., A. P., Eds.; IOP Press, 1995, Vol. 125, pp 491–532

49. Xiangwen, L.; Kebin, Z.; Lei, W.; Wang, B.; Li, Y. Oxygen Vacancy Clusters Promoting Reducibility And Activity Of Ceria Nanorods. *J Am Chem Soc* **2009** 131:3140–3141

50. Wang, L.; Yu Y.; He H.; Zhang, Y.; Qin, X.; Wang, B. Oxygen Vacancy Clusters Essential For The Catalytic Activity Of CeO_2 nanocubes For O-xylene Oxidation. *Sci Rep* **2017** 7:1–11

51. Sachdeva, A.; Chavan, S.V.; Goswami, A.; Tyagi, A.K.; Pujari, P.K. Positron Annihilation Spectroscopic Studies On Nd-Doped Ceria. *J Solid State Chem* **2005** 178:2062–2066

52. Thorat, A.V.; Ghoshal, T.; Holmes, J.D.; Nambissam, P.M.G.; Morris, M.A. A Positron Annihilation Spectroscopic Investigation Of Europium-Doped Cerium Oxide Nanoparticles. *Nanoscale* **2014** 6:608–615

53. Yoshida, H.; Deguchi, H.; Miura, K.; Horiuchi, M.; Inagaki, T. Investigation of the relationship between the ionic conductivity and the local structures of singly and doubly doped ceria compounds using EXAFS measurement. *Solid State Ionics* **2001** 191-199

54. Deguchi, H.; Yoshida, H.; Inagaki, T.; Horiuchi, M. EXAFS study of doped ceria using multiple data set fit. *Solid State Ionics* **2005** 1817-1825

55. Barsan, N.; Weimar, U. Fundamentals Of Metal Oxide Gas Sensors. *The 14th Int Meet Chem Sensors* **2012** 618–621

56. Zacherle, T.; Schriever, A.; De Souza, R.A.; Martin, M. Ab Initio Analysis Of The Defect Structure Of Ceria. *Phys Rev B* **2013** 87:134104

TOC Graphic